DISTRIBUTION STATEMENT A. Approved for public release; distribution is unlimited.

Fluctuations of Broadband Acoustic Signals in Shallow Water

Mohsen Badiey
College of Earth, Ocean, and Environment
University of Delaware
Newark, DE 19716
Phone: (302) 831-3687 Fax: (302) 831-3302 Email: badiey@udel.edu

Award Number: N00014-10-1-0396
http://oalab.cms.udel.edu

LONG-TERM GOALS

The long-term goal of this project is to obtain quantitative understanding of the physical mechanisms governing broadband (50 Hz to 50 kHz) acoustic propagation, reflection, refraction, and scattering in shallow water and coastal regions in the presence of temporal and spatial ocean variability.

OBJECTIVES

The scientific objective of this research is to understand acoustic wave propagation in a dynamic environment in two frequency bands: Low (50 Hz to 500 Hz) and Mid-to-High (500 Hz to 50 kHz). The goal for the low frequency band is to assess the effects of internal waves on acoustic wave propagation, with an emphasis on the mechanisms that cause significant temporal and spatial acoustic intensity fluctuations. The goal for the mid-to-high frequency band is to assess the effects of water column and dynamic sea surface variability, as well as source/receiver motion on acoustic wave propagation for underwater acoustic communications, tomography, and other applications.

APPROACH

The project combines theoretical, experimental, and modeling efforts to improve our understanding of broadband acoustic wave propagation in a dynamic shallow water environment. Studies in the low frequency band have been focused on the data from the SW06 experiment for both stationary [1] and moving sources with vertical and horizontal array receivers. A 3D acoustic propagation model has been utilized and a detailed 3D environment data required as input to the model has been constructed using temperature and radar image data. Improvement has been made with better estimation of the internal wave front curvature and better estimation of the receiver positions.

Studies in the mid-to-high frequency band have utilized data collected at KAM08 [2] and KAM11 [3] experiments. The effects of sea surface, including surface bubbles, and water column variability on acoustic wave propagation have been investigated using Parabolic Equation (PE) model. A time evolving nonlinear sea surface wave model is being developed to realistically simulate the sea surface and wave breaking to determine the location of surface bubbles generation. To take into account the out-of-plane acoustic scattering and the directionality of the surface wave, the PE acoustic propagation model is being extended to 3D.

Report Documentation Page

Form Approved
OMB No. 0704-0188

Public reporting burden for the collection of information is estimated to average 1 hour per response, including the time for reviewing instructions, searching existing data sources, gathering and maintaining the data needed, and completing and reviewing the collection of information. Send comments regarding this burden estimate or any other aspect of this collection of information, including suggestions for reducing this burden, to Washington Headquarters Services, Directorate for Information Operations and Reports, 1215 Jefferson Davis Highway, Suite 1204, Arlington VA 22202-4302. Respondents should be aware that notwithstanding any other provision of law, no person shall be subject to a penalty for failing to comply with a collection of information if it does not display a currently valid OMB control number.

1. REPORT DATE	2. REPORT TYPE	3. DATES COVERED
2012	**N/A**	**-**

4. TITLE AND SUBTITLE	5a. CONTRACT NUMBER
Fluctuations of Broadband Acoustic Signals in Shallow Water	5b. GRANT NUMBER
	5c. PROGRAM ELEMENT NUMBER
6. AUTHOR(S)	5d. PROJECT NUMBER
	5e. TASK NUMBER
	5f. WORK UNIT NUMBER
7. PERFORMING ORGANIZATION NAME(S) AND ADDRESS(ES) **College of Earth, Ocean, and Environment University of Delaware Newark, DE 19716**	8. PERFORMING ORGANIZATION REPORT NUMBER
9. SPONSORING/MONITORING AGENCY NAME(S) AND ADDRESS(ES)	10. SPONSOR/MONITOR'S ACRONYM(S)
	11. SPONSOR/MONITOR'S REPORT NUMBER(S)

12. DISTRIBUTION/AVAILABILITY STATEMENT
Approved for public release, distribution unlimited

13. SUPPLEMENTARY NOTES
The original document contains color images.

14. ABSTRACT

15. SUBJECT TERMS

16. SECURITY CLASSIFICATION OF:			17. LIMITATION OF ABSTRACT	18. NUMBER OF PAGES	19a. NAME OF RESPONSIBLE PERSON
a. REPORT	b. ABSTRACT	c. THIS PAGE			
unclassified	**unclassified**	**unclassified**	**SAR**	**11**	

WORK COMPLETED

1) *Low Frequency Acoustic Wave Propagation*
A 3D PE model and a detailed 3D environment, reconstructed based on shipboard radar images and temperature data [4], are developed to study both stationary and moving sources propagation scenario with vertical and horizontal array receivers in the presence of internal waves. The model-data agreement was considerably improved when the curvature of the internal wave fronts was included in the model compared to straight wave front assumption [5]. The model was further improved by utilizing better estimation of the internal wave curvature and receiver locations. It is shown that the model not only can reproduce the mechanisms (focusing-defocusing, interference, etc.) of the acoustic intensity fluctuation, but is also able to quantitatively predict the time and location of specific details given a high quality reconstruction of 3D environment as parameter.

2) *Mid-to-High Frequency Acoustic Wave Propagation*
We have continued our analyses of data from KAM08 and KAM11 to assess the effects of the environment on the acoustic wave propagation. For modeling, time-evolving rough sea surfaces used as boundaries in the PE model were re-generated using waverider buoy data from KAM08 and KAM11. A surface bubble generation model was developed and included in the PE model to study the effects of surface bubble on acoustic propagation [6]. Results from the PE model compared well with data and specific features relevant to the acoustic communication research are being studied in detail.

RESULTS

A. Low Frequency Acoustic Wave Propagation in the Presence of Shallow Water Internal Waves

1. Angular dependency (moving source)

During the SW06 experiment in New Jersey shelf, an acoustic source (J15 projector) was towed by the R/V Sharp while following the front of an internal wave packet [1]. The source was transmitting broadband acoustic signals (50-450 Hz) in different angles with respect to the internal wave front in five transmission zones. Signals received on WHOI Vertical and Horizontal Linear Arrays were analyzed and modeled.

For modeling, a 3D environment was reconstructed based on the shipboard radar images of R/V Sharp and R/V Oceanus and temperature data collected on three thermistor strings [4]. Here, the environment model was improved from the previous one by utilizing better estimation of internal wave front curvature and better estimation of the receiver positions. Using the output from this new environment model, the 3D acoustic PE model yielded better agreement with the observations in the SW06 experiment.

Fig. 1(a) shows the new and old model-data comparison of depth-integrated intensity of the received acoustic signal on the vertical array for the second half of Zone 2 transmission (from 21:52 to 22:00 GMT). With the new environment model, the improvement of the PE results is clear at the second half of Zone 2 transmission where the nominal incident angle is about 0^o - 0.5^o. The new model is capable of predicting the intensity focusing at ~21:53 GMT with good agreement of the peaking time as well as the rate of increasing and decaying. To improve the performance of the environment and PE model for

the region of smaller incident angle (the first half of Zone 2 from 21:40 to 21:52 GMT), a Monte Carlo method was adapted, where the shape of the internal wave fronts was randomly perturbed by a small amount. The mean and the +/− standard deviation of the results of 201 model runs are plotted in Fig. 1(b). The data curve generally falls in between the span of two standard deviation lines; however, the model failed to capture the bump of approximately 2 dB happened at around 21:47 GMT, which may due to the insufficient spatial sampling of the temperature field.

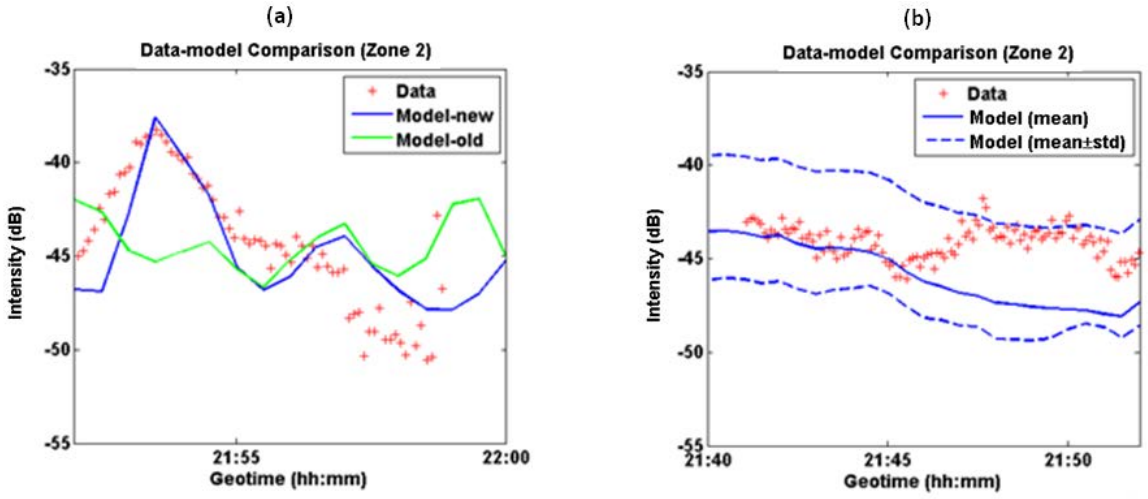

Figure 1: (a) Data-model comparison for Zone 2 from 21:52-22:00 GMT. The improved-model better predicts the sharp peak (focusing) at 21:53, the small dipping at ~21:56, and the drop-off of 8 dB after 21:55. (b) Data-model comparison for Zone 2 from 21:40-21:52 GMT. Plot shows the mean of 201 Monte Carlo simulations and the span of one standard deviation.

2. Analysis of horizontal array data

The acoustic data received on the horizontal leg of Shark array during SW06 experiment have been analyzed and modeled. With newly improved 3D PE model, it is possible to model the horizontal incident ray refracted by the curved internal wave fronts with great detail and accuracy under various conditions. The simulated results show good agreement with the measurements.

Fig. 2 shows acoustic beamforming plots using the acoustic data received on the horizontal leg of Shark array. The arrival time versus incident angle before the internal wave arrived at the receiver is shown in Fig. 2(a). Notice the dominant ray comes at about 65^{o}. Fig. 2(b) shows the same plot for the time period when the major part of the source-receiver track was intersecting with the internal wave packet. The incident angle of the dominant ray has increased to about 85^{o} at about 0.25 sec (relative time), and the second ray comes at 0.17 sec and 65^{o}.

Fig. 3 shows the 3D model results of depth-integrated acoustic intensity with detailed internal wave environment. A 3 km by 3 km square close to the Shark receiver array is shown, with the red line indicating the position and the length of the horizontal leg of Shark array. The source is located at (0,0)

(not shown in the figure). Fig. 3(a) shows the PE model results for the environment before the internal waves arrived (20:30 GMT). At this geotime, the environment was almost homogeneous, resulting in an evenly-distributed acoustical field. The horizontal ray propagates directly from the source to the receiver array with an incident angle about 65^o (corresponding to "1" in Fig. 2a). Fig. 3(b) shows the same plot with the internal waves present (22:00 GMT). From the output of the PE model, two incoming rays are shown arriving at the receiver array, a weak one at about the direction of the source, corresponding to the arrival at 0.17 sec and 65^o (marked as "2" in Fig. 2b), and a strong incoming ray, refracted by the internal wave fronts, corresponding to the arrival at 0.25 sec and 85^o (marked as "3" in Fig. 2b).

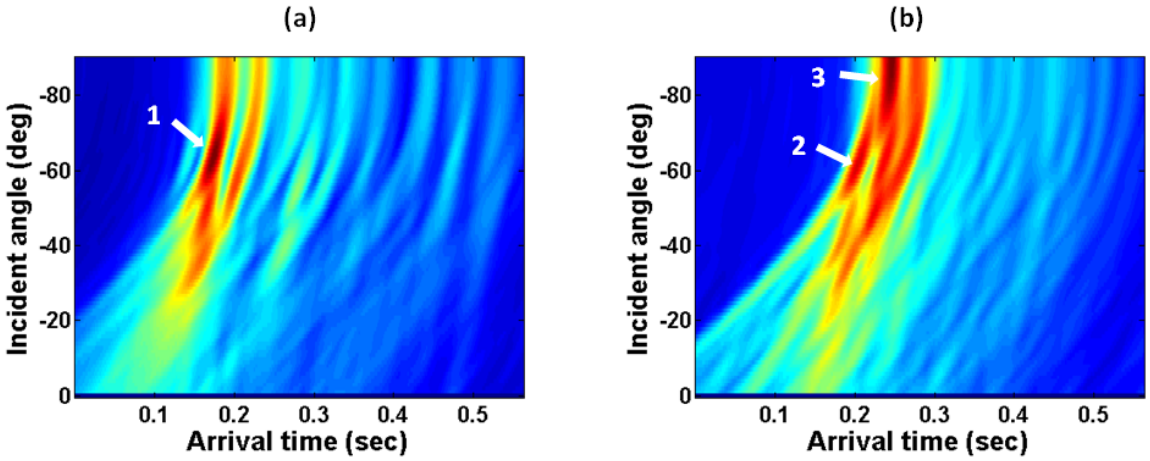

Fig. 2: Acoustic beamforming plots using the acoustic data received on the horizontal leg of Shark array during SW06. (a) The arrival time-versus-incident angle plot before the internal wave arrived. Notice the dominant ray comes at about 65^o (marked as "1"). (b) The same plot for the time period when the majority of the source-receive track was intersecting with the internal wave packet. The incident angle of the dominant ray has increased to about 85^o at about 0.25 sec (relative time) (marked as "3"), and the second ray comes at 0.17 sec and 65^o (marked as "2").

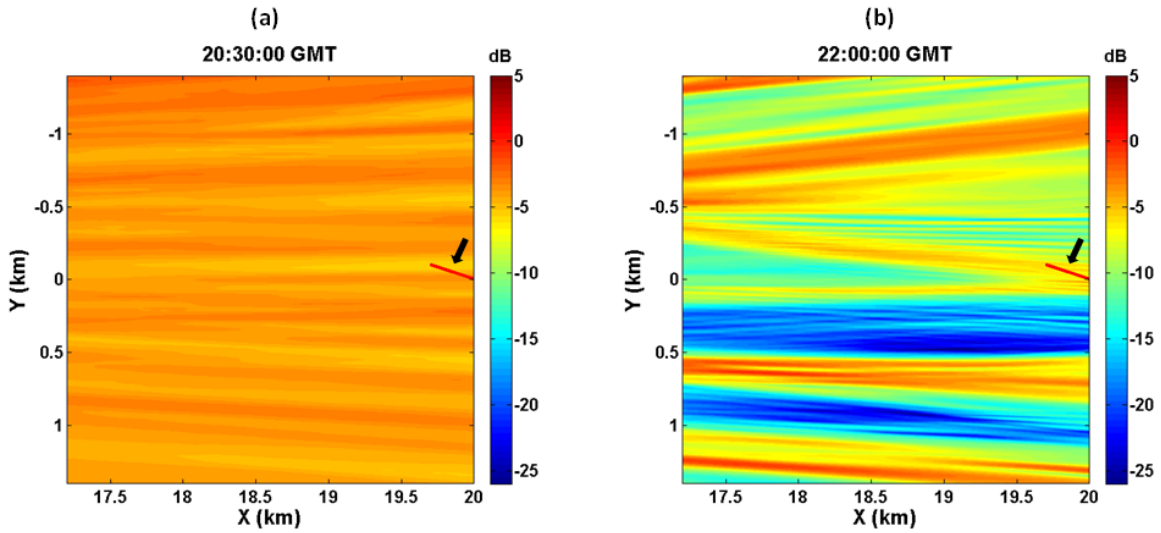

Fig. 3: 3D PE model results of depth-integrated acoustic intensity with detailed internal wave environment. A 3 km by 3 km square close to the Shark receiver array is shown, with the red line (see black arrow) indicating the position and the length of the horizontal leg of Shark array. The source is located at (0,0) (not shown in the figure). (a) Before the internal wave packet arrived (20:30 GMT); the environment was almost homogeneous, resulting in an evenly-distributed acoustical field. The horizontal ray propagates directly from the source to the receiver array with an incident angle about 65^o (corresponding to "1" in Fig. 2a). (b) The internal wave packet was present (22:00 GMT). Two incoming rays arrived at the receiver array: a weak one at about the direction of the source, corresponding to the arrival at 0.17 sec and 65^o ("2" in Fig. 2b), and a strong one, refracted by the internal wave fronts, corresponding to the arrival at 0.25 sec and 85^o ("3" in Fig. 2b).

B. Mid-to-High Frequency Acoustic Propagation in Shallow Water

Surface waves are among several environmental parameters that can have significant influence on acoustic propagation in shallow water. To study the effects of surface wave roughness including the effects of bubbles and surface wave directionality, we have developed 2D and 3D PE acoustic propagation models in conjunction with a 3D time-evolving sea surface boundary to analyze the results obtained during a highly calibrated field KAM11 experiment. In this section we present our results from our recent modeling efforts.

1. PE Model with Bubble Effects

The influences of bubbles, which are generated by breaking waves, on the propagation of acoustic in the ocean depend on the acoustic wave length and the bubble radius. The effects are made more complicated by the presence of a variety of bubble sizes and the varying distribution of bubbles over range and depth [6]. Monahan and Lu [7] developed a classification scheme for bubbles, defining alpha, beta, and gamma plume structures, as well as a background bubbly layer. Fig. 4(a) shows a comparison of the relative spatial scales of the various plumes; the beta plume at time 0 and gamma

plume at the beta expiration time are shown in red and green, respectively, and the blue plume represents the expanded gamma at the time when it disappears into the background layer.

A bubble generation model was developed and incorporated into the PE model [6]. Fig. 4(b-d) show comparison of intensity as a function of range and depth for single frequency runs computed at 20 kHz for rough surface (RS) PE without bubble effects, RS PE with range-dependent bubbles, and RS PE with range-independent bubbles. For this high frequency acoustic, the difference among these 3 cases is noticeable.

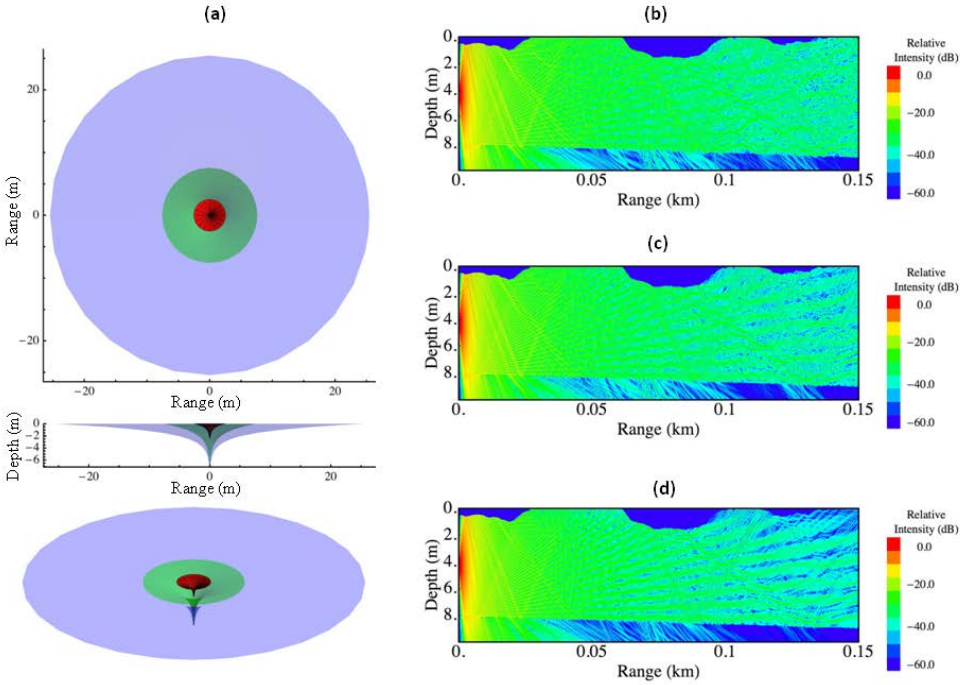

Figure 4: (a) Top, side, and angled views of the relative sizes of a beta plume at initialization (red), a gamma plume at the beta expiration time (green), and a gamma plume at the gamma expiration time (blue), each calculated for a wind speed of 15 m/s. (b) Intensity as a function of range and depth for single frequency runs computed at 20 kHz for RS PE. (c) RS PE with range-dependent bubbles, and (d) RS PE with range-independent bubbles.

Fig. 5(a) shows an example of acoustic data collected during the KAM11 experiment, which exhibited interesting coherent focused surface-interacting structures that are related to the surface wave [6, 8]. The direct and bottom-reflected paths (marked as "1" and "2") exhibited little variation over geotime, whereas the surface and bottom-surface paths (marked as "3" and "4") were highly fluctuating over geotime and remarkably dispersed in arrival time. There were still observable surface returns around arrival time 7-15 ms. Furthermore, there existed intense late coherent surface arrivals, which had decreasing delay over time.

These coherent returns were the result of surface wave crest focusing. Due to the curvature of the surface wave crest, multiple local reflections from the wave crest reached the receiver. With similar arrival time and phases, these reflections created acoustic focusing at the receiver, thus leading to

enhanced intensity [8]. The coherent structure disappeared when the receiver was not in the focusing area of the moving wave crest. During the first several seconds in the geotime axis, multiple coherent returns appeared simultaneously and created a striation pattern of enhanced intensity. This may be the result of acoustic focusing from different wave crests.

The PE runs were able to reproduce the characteristics of the direct and bottom-reflected paths, as well as the features of the surface interacting paths (Fig. 5b-d). The modeled surface-interacting signals dispersed in arrival time and varied over geotime in accordance with the collected data. The PE runs were also able to reproduce the striation patterns that were observed within the dataset. The structure of these patterns is dependent on the directionality of the surface waves. Rough surface PE runs computed with the source-receiver direction reversed showed that the late coherent surface returns had increasing delay over time [8]. This indicates that the directionality of the surface is an important parameter that should be maintained within the surface wave modeling. The ability of the PE to reproduce these directionally dependent patterns further confirmed the usefulness of the model. If only random surfaces were used, one would not be able to track the changes from one geo-time to the next. However, by evolving the surface in time one is able to actively track these coherent returns.

Though there are differences between the outputs of the RS PE, the RS PE involving the range-dependent bubble field, and the RS PE involving the range independent bubble field, these differences are not easily observed within the impulse responses of Fig. 5b-d. Using the ensemble averaging tool, the differences between the runs is minimal. This is in itself due to the fact that the runs were computed at the low end of communications frequencies (10 kHz). The effect of bubbles at low frequencies is to appreciably drop the sound speed, but only slightly increase the attenuation. Consequently, the presence of bubbles in a rough sea surface environment has a minimal effect whenever the acoustic frequencies are sufficiently small.

I. 3D PE Model

To include the out-of-plane acoustic scattering from a rough surface, a 3D model is required. The 3D rough surface PE model using split-step Fourier (SSF) algorithm in cylindrical coordinate has been developed by K.B. Smith [9]. For high frequency acoustic wave and large source-receiver range, this model is not efficient since the radial spatial step is not uniform in range, resulting in less spatial resolution for larger range. Here we are modifying the code to a Cartesian coordinate where the spatial step is uniform.

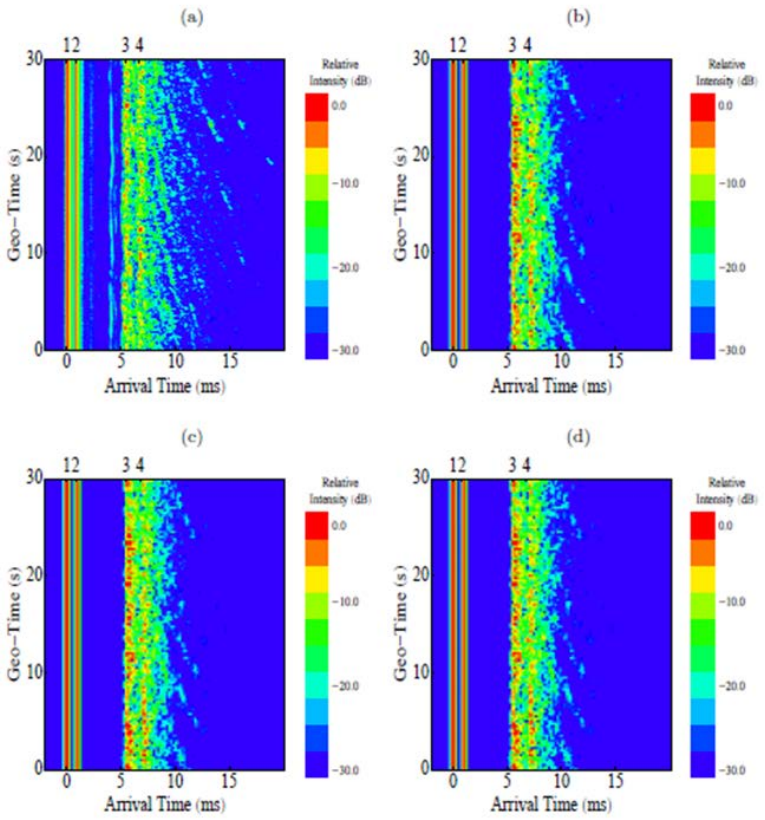

Figure 5: Impulse intensity as a function of arrival time, shown over a 30 s geo-time period. Results shown for (a) data, (b) RS PE, (c) RS PE with range-dependent bubbles, and (d) RS PE with range-independent bubbles. Numbers on top of figures indicate the (1) direct, (2) bottom-reflected, (3) surface-reflected, and (4) bottom-surface-reflected paths.

Fig. 6 shows the 2D PE (Fig. 6a) and 3D PE (Fig. 6a and 6b) results for a case of a planar sinusoid sea surface with 20 m wave height and 200 m wavelength. The acoustic frequency is 500 Hz, source-receiver range is 2 km, water depth is 100 m, and the source depth is 30 m. The 3D Cartesian model is still under construction and need to be verified and compared with a benchmark case.

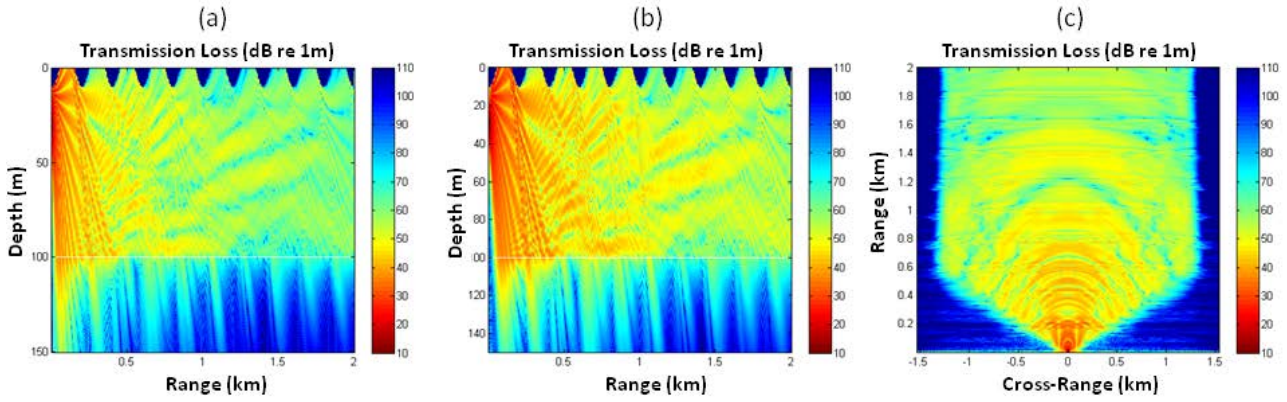

Figure 6: Comparison between 2D PE and 3D PE for case of planar sinusoid sea surface with wave height=20m and wavelength=200m. The acoustic frequency is 500 Hz, source-receiver range is 2km, water depth is 100m, and the source depth is 30m. (a) 2D acoustic field: range vs. depth. (b) 3D acoustic field: range vs. depth. (c) 3D acoustic field: range vs. cross-range at 30 m depth.

II. Nonlinear Surface Wave Model

Time evolving 3D nonlinear surface wave model is being developed to simulate the sea surface realistically. The model is an extension of the work by Xu and Guyenne [10] to include wave breaking. The extended-model gives the locations of breaking waves in the surface field, which related to the location of bubble origins. Breaking criteria to detect breaking events and detail of the model can be found in [11]. Fig. 7(b) plots an example of sea surface realization generated by the 3D nonlinear surface model using wave spectrum from KAM 11 experiment (shown in Fig. 7a). The locations of the breaking on the surface field are shown as red dots in Fig. 7(c). This information is then used in the bubble generation model to calculate the time and spatial dependent of sound speed and attenuation for the PE acoustic propagation model.

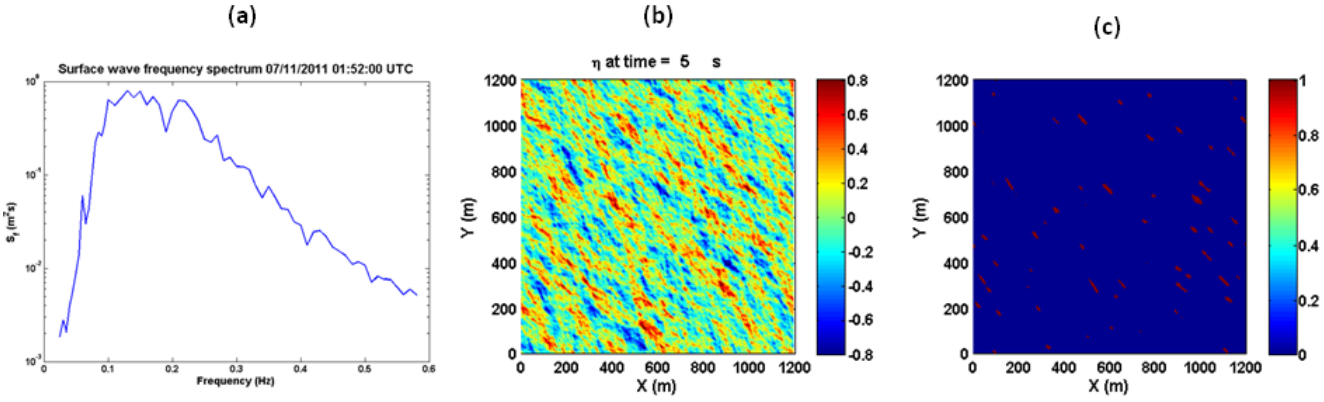

Figure 7: Time evolving nonlinear surface wave model. (a)KAM11 frequency spectrum on July 11, 2011 at 01:52:00 UTC is used to generate surface wave initial field. (b) Sample of surface field at time=5s. (c) Plot of the locations of breaking on the surface field for input to the bubble generation model.

IMPACT/APPLICATIONS

The low frequency component of our research contributes to the understanding of acoustic propagation in complex shallow water regions. We have developed a model that is able to reproduce the mechanism of acoustic intensity variation due to internal waves and to quantitatively predicts the time and location of specific details. The high frequency part of our research has contributed to the understanding of the effects of surface wave roughness and directionality as well as bubble effects on sound propagation, which in turn affect the performance of acoustic communication signals.

RELATED PROJECTS

In our low frequency band research, we have been working with Dr. J. Lynch from Woods Hole Oceanographic Institute (WHOI) and Dr. B. Katsnelson from University of Voronezh, Russia. For the research work in the high frequency band, we are collaborating with Dr. W. Hodgkiss and Dr. H.-C. Song from Scripps Institution of Oceanography, Dr. K. B. Smith from Naval Post Graduate School, and Dr. M. Porter from Heat, Light, and Sound Research Inc.

REFERENCES

[1] J. Luo, M. Badiey, E. A. Karjadi, B. Katsnelson, A. Tskhoidze, J. F. Lynch, and J. N. Moum, "Observation of sound focusing and defocusing due to propagating nonlinear internal waves," *J. Acoust. Soc. Am.*, 124(3), EL66–EL72, September 2008.

[2] W. S. Hodgkiss, *et al.*, "Kauai Acomms MURI 2008 (KAM08) Experiment Trip Report," July, 2008.

[3] W. S. Hodgkiss, *et al.*, "Kauai Acomms MURI 2011 (KAM11) Experiment Trip Report," August, 2011.

[4] J. Luo, M. Badiey, and Y-T. Lin, "Horizontal focusing/defocusing due to shallow-water internal waves," *POMA*, Vol. 9, 2010.

[5] J. F. Lynch, Y.-T. Lin, T. F. Duda, A. E. Newhall, and G. Gawarkiewicz, "Acoustic ducting, refracting, and shadowing by curved nonlinear internal waves in shallow water," *J. Acoust. Soc. Am.*, 125, 2591, 2009.

[6] J. Senne, "High Frequency Acoustic Propagation under Variable Sea Surfaces," Ph.D. Dissertation, University of Delaware, Newark, Delaware, 2012.

[7] E. C. Monahan and M. Lu, "Acoustically relevant bubble assemblages and their dependence on meteorological parameters," *J. Ocean. Eng.*, 15(4), 340-349, 1990.

[8] M. Badiey, A. Song, and K. B. Smith, "Coherent reflection from surface gravity water waves during reciprocal acoustic transmissions," *J. Acoust. Soc. Am.,* 132(4), EL290-EL295, 2012.

[9] K. B. Smith, "Field transformational approach of three-dimensional scattering from two-dimensional rough surface," *J. Acoust. Soc. Am.*, 131(6), EL1–EL7, June 2012.

[10] L. Xu and P. Guyenne, "Numerical simulation of three-dimensional nonlinear water waves," *J. Computational Physics*, 228, 8446-8466, 2009.

[11] N. Pophet, "Parallel implementation of a three-dimensional nonlinear wave model for random directional seas," Master's thesis, University of Delaware, 2012.

PUBLICATIONS

[1] M. Badiey, A. Song, and K. B. Smith, "Coherent reflection from surface gravity water waves during reciprocal acoustic transmissions," *J. Acoust. Soc. Am.,* 132(4), EL290-EL295, 2012.

[2] J. Senne, A. Song, M. Badiey, and K. B. Smith, "Parabolic equation modeling of high frequency acoustic transmission with an evolving sea surface," *J. Acoust. Soc. Am*., 132(3), 1311-1318, 2012.

[3] E. A. Karjadi, M. Badiey, J. T. Kirby, and C. Bayindir, "The effects of surface gravity waves on high frequency acoustic propagation in shallow water," *J. Ocean. Eng*., 37(1), 112-121, 2012.

[4] J. Luo and M. Badiey, "Frequency dependent beating patterns and amplitude increase during the approach of an internal wave packet," *J. Acoust. Soc. Am*., 131(2), EL145-EL149, 2012.

[5] A. Song and M. Badiey, "Time reversal multiple-input/multiple-output acoustic communication enhanced by parallel interference cancellation," *J. Acoust. Soc. Am.,* 131(1), 281-291, 2012.

[6] A. Song and M. Badiey, "Time reversal acoustic communication for multiband transmission," *J. Acoust. Soc. Am.,* 131(4), EL283-EL288, 2012.

M. Badiey, B. G. Katsnelson, Y.-T. Lin, and J. F. Lynch, "Acoustic multipath arrivals in the horizontal plane due to approaching nonlinear internal waves," *J. Acoust. Soc. Am.,* 129(4), EL141-EL147, doi: 10.1121/1.3553374, 2011.